Q. J. R. Meteorol. Soc. (2003), **129**, pp. 1903–1927 doi: 10.1256/qj.02.04

Initial stages in the morphological evolution of vapour-grown ice crystals: A laboratory investigation

By NEIL J. BACON[1], MARCIA B. BAKER[2] and BRIAN D. SWANSON[2*]

[1]*Department of Physics, University of Washington, USA*

[2]*Department of Earth and Space Science, University of Washington, USA*

(Received 10 January 2002; revised 14 December 2002)

SUMMARY

We describe experiments to investigate the first stages in the evolution of small (100–200 μm) ice crystals levitated in air at temperatures and humidities characteristic of fully glaciated stratiform clouds. We find that in these conditions particle morphology is not uniquely determined by environmental temperature and humidity as has commonly been assumed; other parameters, such as the mode of ice initiation, appear to have important effects on particle shape. Crystals grown from frozen droplets at vapour excesses of less than about 0.05 g m^{-3} adopt isometric compact habits at temperatures above -22 °C, while polycrystals dominate at lower temperatures. In contrast, crystals grown under similar conditions from frost 'seeds' usually develop into pristine hexagonal prisms with varying aspect ratios. An increasing fraction of frozen droplets develop into 'florid' crystals, containing thin side-planes, at higher supersaturations. This mix of particle types is similar to that found in field studies of cold clouds. The change in morphology from compact hexagon to 'florid' with increasing growth rate defines a facet instability transition, from which we infer a lower limit for the critical supersaturation for layer nucleation on the prism facet to be 2.4% at -15 °C and 3.1% at -25 °C. We develop a simple analytic model for the size dependence of facet stability and show its predictions compare well with the data.

KEYWORDS: Electrodynamic balance Facet instability Habit Ice-crystal growth Morphological phase transition

1. INTRODUCTION

The earth's climate is extremely sensitive to the microphysical properties of fully glaciated stratiform clouds in the troposphere (Vogelmann and Ackermann 1995; IPCC 2001), in which the temperatures are often below -25 °C, and water-vapour densities and supersaturations with respect to ice are low. Field studies show that, in these clouds, most of the ice crystals are smaller than 200 μm, particularly at low ice-water content (Arnott *et al.* 1994; McFarquhar and Heymsfield 1996; Korolev and Isaac 1999; Matrosov and Heymsfield 2000; Shupe *et al.* 2001) and these small crystals are thought to dominate the cloud optical properties (Stephens *et al.* 1990). Moreover, recent advances in instrumentation (Lawson *et al.* 1998; Korolev and Isaac 1999; Shupe *et al.* 2001) have made it possible to image particles more accurately than ever before, revealing that the ice particles in these clouds often have complex irregular shapes; relatively few have the pristine hexagonal prism-shaped habits characteristic of the ice crystals examined in many earlier laboratory studies.

The response of ice-particle shape to environmental conditions has been the focus of a number of studies dating back to the 1950s. Most laboratory habit studies to date have focused on temperatures higher than -22 °C, and the environment in mixed-phase clouds, where the humidity is maintained at water saturation and the ice crystals grow to millimetre scale in tens of minutes (Hallett and Mason 1958; Fukuta and Takahashi 1999). Although some theoretical treatments (Frank 1982; Yokoyama and Kuroda 1990; Nelson and Baker 1996; Wood *et al.* 2001, and others) have proposed constraints on stable growth, these have not been applied to the laboratory observations or to particles observed in clouds. Thus, we do not have a clear picture of the factors that produce the kinds of ice particles prominent in glaciated stratiform clouds in the atmosphere.

* Corresponding author: Department of Earth and Space Science, University of Washington, Seattle, Washington, 98195, USA. e-mail: brian@ess.washington.edu

In the present study, our goal is to investigate the environmental parameters that most strongly influence shape characteristics and morphological stability of 30–200 μm ice crystals grown under conditions typical of those in fully glaciated, boundary-layer glaciated clouds. Our particular focus is the delineation of the conditions that lead to compact hexagonal crystals versus those that instead lead to polycrystals or irregular single crystals. Our study is one of the first to concentrate on the effects of the nucleation process on particle habit and we chose to simplify the situation by doing all experiments at sea-level pressure. Extension to clouds in the lower-pressure regimes of the troposphere is planned for a future study.

2. Ice-crystal shapes and facet instabilities; previous results

(*a*) *Primary habit*

We define the primary habit of a crystal by its aspect ratio $\Gamma = (c/a)$, where for a hexagonal column, the column height is $2c$ and the hexagonal basal-facet corner-to-corner width is $2a$. Variation with temperature of the aspect ratios of ice crystals grown at high ambient supersaturation has been well documented in both field and laboratory studies (Nakaya 1954; Shaw and Mason 1955; Hallett and Mason 1958; Kobayashi 1961; Heymsfield 1973; Rottner and Vali 1974; Ryan *et al.* 1976; Gonda 1977; Colbeck 1983; Takahashi and Fukuta 1988; Sei and Gonda 1989; Fukuta and Takahashi 1999). It is not our intention here to make detailed or complete comparisons of the many measurements that have been made; however, we have analysed the qualitative findings of several studies of ice-crystal aspect ratios in field, laboratory cloud chamber, fibre, and substrate-based experiments (Nakaya 1954; Shaw and Mason 1955; Hallett and Mason 1958; Kobayashi 1961; Ono 1970; Gold and Power 1971; Heymsfield 1973; Rottner and Vali 1974; Ryan *et al.* 1976; Gonda 1977; McKnight and Hallett 1978; Auer and Veal 1979; Keller *et al.* 1980; Colbeck 1983; Sei and Gonda 1989; Takahashi *et al.* 1991; Fukuta and Takahashi 1999). In most cases, the particles were grown from frozen droplets, and their masses had grown by factors of a thousand or more after the initial ice particles were formed. Overall, there is no noticeable dependence of Γ on the type of experiment (i.e. fibre, cloud chamber, substrate, or field study). While supersaturations were not always given in the papers describing the measurements, it appears that the major features of this compilation are as follows: (i) for vapour-density excess of greater than around 0.10 g m^{-3} (i.e. supersaturation relative to ice of about 4.7% at a temperature $T = -10\,^{\circ}$C) the habit alternates between clearly columnar and clearly plate like, whereas for lower supersaturations the crystals were more isometric at all temperatures, but (ii) there is scatter throughout the temperature range, even when the data are sorted by growth rate and even in data reported for a given experimental arrangement. For example, Kobayashi (1961) grew both plates and columns at $-15\,^{\circ}$C, while Shaw and Mason (1955) reported high variability of Γ in their crystals over a wide range of temperature. The reasons for this variability were not discussed and little or no mention was made of irregular or complex crystal shapes.

(*b*) *Facet instability*

Polyhedral crystal growth can manifest a phenomenon referred to as a facet instability. This process, distinct from the dendritic transition at high supersaturation, occurs either on basal faces resulting in hollowed columns, or on prism faces resulting in the formation of side planes. We have used the term 'florid' to characterize crystals with side planes whose crystalline axes appear to be the same throughout the particle (thus indicating these are probably single crystals). Side planes were identified by Magano and

Lee (1966) under the classification S1, S2, and S3; the same authors identified columns with plates (CP1, CP2) that exhibit similar thin plate-like extensions. Such morphologies were reported in field studies at temperatures below $-20\,^{\circ}$C: McFarquhar and Heymsfield (1996) observed side planes in tropical cirrus clouds of high ice-water content, suggestive of a correlation with high supersaturation. Nakaya noted them in crystals grown between $-20\,^{\circ}$C and $-30\,^{\circ}$C (see pp. 287–293 of Nakaya 1954). Double-plate crystals have been observed in both the laboratory and field (Veal 1954; Heymsfield 1973) and seem to be associated with growth from frozen droplets.

Ice-crystal growth models (e.g. Kuroda and Lacmann 1982; Yokoyama and Kuroda 1990; Yokoyama 1993; Wood *et al.* 2001) predict that facet instability depends on crystal size and the growth mechanism, (i.e. dislocation or layer-nucleation-mediated growth). The predicted trends are observed in recent field studies (e.g. Korolev and Isaac 1999; Korolev *et al.* 2000) which show that small crystals $<50\ \mu$m are often compact hexagons, while larger particles tend to exhibit complex morphologies. Gonda and his co-workers have observed strong size dependence of facet instability (Gonda and Koike 1982; Gonda and Yamazaki 1982; Gonda and Koike 1983) at both $-15\,^{\circ}$C and $-30\,^{\circ}$C. They found that crystals on a substrate underwent facet instability as they grew larger than about 25 μm in size at approximately 10% supersaturation and at $-15\,^{\circ}$C. The instability has not been studied in crystals growing in air at low supersaturations.

In this paper we compare observed and predicted values of the supersaturations and crystal sizes at which facet instability occurs. We use our observations to infer the dominant growth mechanisms and the critical supersaturation for layer nucleation, $\sigma_{2D}(T)$, previously measured only in the case of ice grown on substrates (Shaw and Mason 1955; Nelson and Knight 1998). Our aim is to explore this transition in the absence of a substrate and to investigate the determining factors for morphological instability.

The new instrument we have designed for these studies is described briefly in section 3, where we outline our experimental procedure. Our experimental results are summarized in section 4; we analyse them in section 5; we present a model for the facet instability in section 6; our conclusions and discussion of implications end the paper.

3. Experimental apparatus and procedure

In this study, our goal was to understand the physical processes determining the initial stages of evolution of atmospheric ice particles. Therefore, we wish to follow individual particles in time rather than to study the evolution of populations of particles in a cloud chamber. The technique of electrodynamic trapping affords us the opportunity to hold and carefully observe a single well characterized liquid or solid particle for *in situ* study without the use of substrates. While this technique yields no information on ventilation effects and cannot capture particle–particle interactions, it is well suited for our study of small ice particles. A detailed description of the application of electrodynamic levitation to the study of cloud microphysics in an earlier humidity-controlled balance can be found in Swanson *et al.* (1999).

(*a*) *The low-temperature, humidity-controlled, electrodynamic balance*

An electrodynamic balance (EDB) levitates and stabilizes charged particles in free space using superposed direct current (DC) and alternating current (AC) fields. Details of the new EDB, constructed specifically for low-temperature studies of ice and used for most of the experiments reported in this paper, are described more fully in Swanson *et al.* (submitted to *Rev. Sci. Inst.*). We provide here only a cursory summary of its operation.

In the new EDB, the particle is trapped at the centre of a temperature-controlled and vacuum-sealed thermal diffusion chamber (TDC). The overall cooling of the balance chamber is provided by a temperature-controlled bath (Neslab ULT-80) which circulates cryogen inside the walls of the chamber. The balance chamber is surrounded by a vacuum jacket with an octagonal cross-section containing optical windows for light illumination, video-telemicroscopy and angular light-scattering measurements. The top and bottom of the chamber are sealed with a sliding valve and fitted with removable optical windows for additional optical access, particle injection and chamber access. A cylindrical window around the balance chamber 'waist' seals the chamber from the surrounding vacuum jacket and provides optical access to the chamber. Temperature monitoring and control is provided by thermistors mounted in each endcap, in the stainless-steel walls above and below the cylindrical window, and near the centre of the cylindrical quartz window itself. A pair of ring electrodes situated near the centre of the balance chamber are connected to specially designed electronic circuitry that provides a variable-frequency high-voltage AC potential superposed on a DC levitating potential difference.

Because the ice particles we study are non-spherical, their sizes cannot be readily measured from their light-scattering properties, so instead, we use a combination of electronic mass and optical size and shape measurements. The electronic mass measurements are made using a technique described by Davis and co-workers (Davis *et al.* 1990; Swanson *et al.* 1999). We measure the particle sizes and shape optically using two video cameras situated 90° apart and fitted with telemicroscopic lenses. The images, obtained from the two cameras with backlit pulsed light-emitting-diode illumination, are combined side by side using a screen splitter before passing to the video monitor, computerized frame-grabber system and video recorder. In the present study, we calibrated the size measurement using water droplets whose sizes were measured optically and found the overall accuracy of the effective size measurements to be about ±5%. Optical measurements have a resolution limit in our system of about ±2 μm.

(*b*) *Ice initiation and growth*

Model studies of ice formation in the atmosphere (Chen and Lamb 1999; Khvorostyanov and Curry 2000; Ovtchinnikov and Kogan 2000) distinguish between 'vapour deposition' on aerosol particles (vapour to a solid state without the intermediary of liquid water), and 'freezing' (liquid to a solid state). Freezing is called 'condensation freezing' for aerosol solution droplets in equilibrium at relative humidities below 100%, and is called 'droplet freezing' for dilute cloud droplets near or above 100% relative humidity. In our experiments the humidity never rises to water saturation, so the process we refer to here as 'droplet freezing' is the freezing of droplets that are evaporating slightly. This situation corresponds to that found by Field *et al.* (2001) and others (DeMott *et al.* 1998; Rangno and Hobbs 2001) to be propitious for ice formation in atmospheric clouds.

We studied the effects of the ice initiation process on final particle shape by starting with three types of initial particle—liquid droplet, frost particle and frost 'seed'. While these do not exhaust the scenarios in which ice particles form in the atmosphere, they represent a reasonable range for this initial investigation.

(i) *Droplet injection and freezing.* We used two methods for droplet generation. In one, we applied a high-voltage pulse (5 kV) to a syringe needle containing water, causing the meniscus to burst and eject droplets with a range of sizes 30–60 μm charged to about 0.5 pC. In the other method, a droplet generator from an inkjet cartridge (supplied by Hewlett Packard) was interfaced with a pulse-generation circuit.

This produced droplets of radius about 20 μm either singly or in a continuous stream. We charged the droplets inductively by means of a grid at -500 V approximately 1 mm from the nozzle plate. The charge induced on the particle was of the order of 0.1 pC. The sliding valve at the chamber top was opened to introduce the charged water droplet generated by one of the two methods described above. We detected the trapped droplet optically and adjusted the DC voltage and AC voltage and frequency to achieve stable trapping.

In the experiments, in addition to the growth temperature and growth rate, we varied both the freezing temperature and the freezing mode. For low-temperature ice initiation, pure high-pressure liquid chromatography (HPLC)-grade water droplets were injected (prior to heating the upper endcap) at chamber temperatures below $-35\,^{\circ}$C. After trapping and freezing, the top plate was heated, and the temperature stabilized to the growth temperature after a few minutes. These particles were grown mostly below $-30\,^{\circ}$C. We term this process 'homogeneous ice initiation' since such droplets remained liquid when injected into a warmer chamber (above $-35\,^{\circ}$C). Heterogeneous droplet freezing was induced at higher temperatures with the TDC endcap temperatures set appropriately prior to droplet injection using water droplets containing the bionucleant SNOMAX (York Int.) which is derived from the bacteria *pseudomonas syringae 31A* (Vali *et al.* 1976; Welch and Speidel 1989; Liao and Ng 1990). We prepared the initial SNOMAX solution by mixing one pellet (approximately 0.01 g) of dry SNOMAX with a litre of HPLC-grade water. This resulted in about 10^{-13} g of SNOMAX per 20 μm droplet. The cells of *pseudomonas syringae* are micron scale (Welch and Speidel 1989), and such a concentration is consistent with several cells per 20 μm radius droplet.

We identified frozen particles both by shape and by their growth in ice-supersaturated (yet water undersaturated) conditions. Droplets that froze did so almost immediately before the image could be focused, and we did not witness any freezing events in detail. Droplets containing SNOMAX froze at ambient temperatures as high as $-10\,^{\circ}$C as they fell from the injection point to the TDC centre. This is consistent with the results of Liao and Ng (1990). Wood *et al.* (2002) report a mean freezing temperature for similar-sized SNOMAX-containing droplets of about $-9\,^{\circ}$C.

(ii) *Frost-particle introduction.* In our earlier balance (Swanson *et al.* 1999), we observed the growth of frost particles of various initial shapes and sizes. The typical procedure was as follows: each day the EDB chamber was carefully cleaned and the vapour sources were loaded with HPLC water. The chamber was then closed and allowed to equilibrate thermally. Frost formations often nucleated and grew from vapour on the inside of the chamber itself. We trapped irregularly shaped ice crystals in the EDB by opening the chamber, breaking off and then 'flicking' particles from these frost formations into the EDB using a thin stainless-steel needle. The frost particle introduction process typically took a few seconds and then the chamber was closed. These particles carried a net electrostatic charge in the range 0.1–0.5 pC. For these particles, the TDC endcap temperatures were set to the appropriate temperatures for growth prior to particle introduction.

(iii) *'Seed'-initiated ice.* In both our earlier and current EDB, particles of frost with initial irregular shapes were flicked from the frost formations inside the chamber and trapped in the EDB. Subsaturated conditions were then produced near the balance centre by removing infrared filters and infrared mirrors from light beams illuminating the chamber, thereby increasing the temperature of the particle and the surrounding air in the chamber. The frost particle was then allowed to sublimate to a 'seed' of linear dimension less than 10 μm. Once mass changes stopped and a seed was obtained (typically

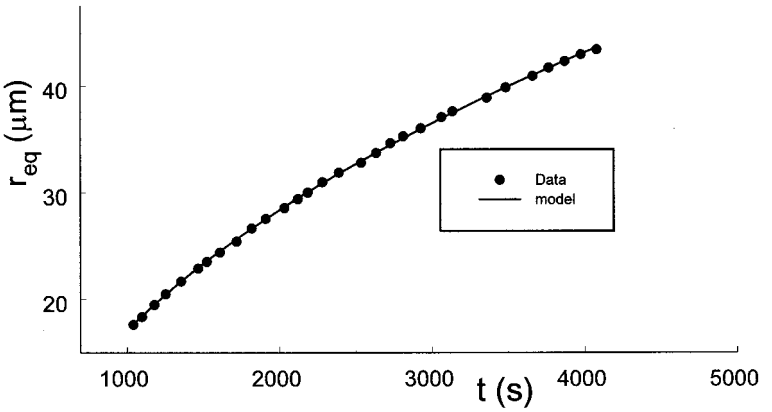

Figure 1. A typical plot of the spherical-equivalent radius (r_{eq}) versus time (in this case for an ice particle growing at −35.1 °C). The line is a fit to the data using a simple model of heat and vapour diffusion to an equivalent sphere, with supersaturation $S = 10.4\%$ with respect to ice. By fitting such growth curves, we can define an effective supersaturation for each run.

after about 20 minutes of sublimation), the seed was usually kept in subsaturated conditions for at least an additional 5 minutes before growth conditions were initiated by elimination of the infrared illumination. Although we could detect no additional decrease in particle mass during this waiting time, we do not know if ice remained in a crack or on the surface of the seed.

(*c*) *Humidity conditions and ice-particle growth*

The saturation ratio at chamber centre was controlled by the temperature difference ΔT between the upper and lower ice surfaces in the TDC. A temperature difference ΔT of at least 15 °C was needed to achieve ice saturation, and we conducted most ice-growth experiments with $\Delta T > 20$ °C. All observations reported here were made at 1 atmosphere pressure in air.

The humidity at the chamber centre could not be derived from the measured chamber temperatures since, in many cases, there were vapour sinks in the vicinity of the particle, evidenced by frost growth on the ring electrodes. The fact that particle growth rates depend on the degree of frost build-up makes *a priori* humidity determination problematic. Instead, we use the measured particle growth rate to deduce the humidity at the chamber centre, fitting data to a simple spherical model for vapour and heat diffusional growth (Swanson *et al.* 1999; Swanson *et al.*, submitted to *Rev. Sci. Inst.*). Figure 1 shows one example of this curve-fitting technique to obtain the environmental supersaturation σ_∞. We see from Fig. 1 that the equivalent-sphere growth model fits the data quite well with only one inferred σ_∞; the variation over a growth curve in this parameter was typically between 0.5 and 2% depending on the growth conditions. While the spherical model neglects shape effects, these are small for our considerations here of mass growth rate, although shape effects may be important for linear growth measurements. (e.g. Wood *et al.* 2001).

When the pure water droplets did not freeze, we measured the evaporation rate to compare with our humidity calibration obtained from the growth or sublimation of ice particles held at the same conditions. The evaporation data tend to be somewhat noisy, since the droplets evaporate rapidly, but the humidity implied by the droplet evaporation data agrees with that deduced from ice-particle growth under similar conditions to within ±2% in saturation (i.e. 0.02 in saturation ratio).

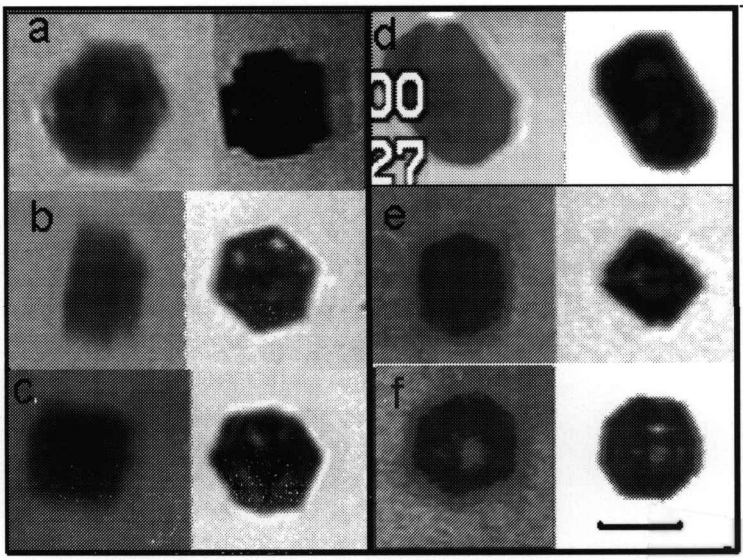

Figure 2. Examples of compact hexagonal ice crystals grown from heterogeneously frozen droplets. Temperatures and supersaturations for each particle shown here range from −14 to −32 °C and 3 to 6%, respectively. As in the other images, each particle is shown from two viewpoints 90° apart. (100 μm scale line for all the images.)

(*d*) *Possible influence of surface charges, external electric fields and trace contaminants*

Strong electric fields (in excess of 5×10^4 V m^{-1}) have been observed to modify ice-crystal habits (Bartlett *et al.* 1963; Evans 1973; Libbrecht and Tanusheva 1998). In the vicinity of our particles the DC field strength was typically $<10^4$ V m^{-1}, and we did not observe the type of dendritic growth that is associated with this effect. Although we can not rule out electric-field effects, we find no noticeable growth rate or morphological differences attributable to variation in particle charge from 0.08 to 0.8 pC. Chernov and Trusov (1969) have shown theoretically that the presence of surface charges may lower the critical supersaturation for layer nucleation σ_{2D}, thereby influencing their habits. However, Chernov did not consider the effect of variations of charge *density*, only the effect of isolated charges, so it is not clear how his result applies to real ice crystals with finite surface charge.

To control potential contamination, the chamber is sealed with o-rings against the circulating cryogen. The choice of o-ring elastomer is constrained by the need for chemical compatibility and low permeability to cryogen vapour, and the elastomer type sets the operable temperature range. To check for habit modification due to trace contaminants we have used various types of cryogenic fluids (some with much lower vapour pressures) to look for habit modification and did not detect any systematic difference in growth morphologies between datasets gathered with different cryogen types.

4. Experimental results: Habit

We followed the evolution of over 100 ice particles at temperatures between −4 and −38 °C and supersaturations between 0 and 10%—always well below water saturation, to a final size of about 100–200 μm. The resulting particle shapes

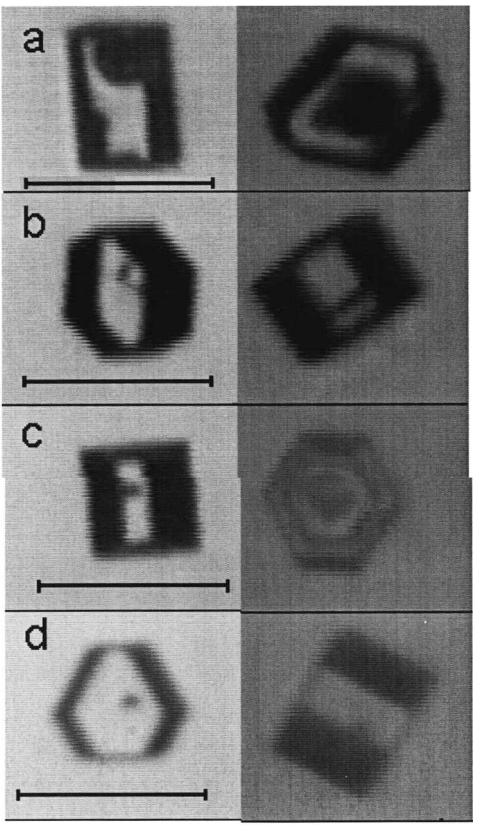

Figure 3. Examples of compact hexagonal ice crystals grown from seeds. Sometimes the hexagon is distorted but note the increased pristine nature and visual clarity of these crystals compared with the hexagonal crystals grown from frozen droplets. The temperatures and supersaturations for each particle shown here range from −5 to −25 °C and 1 to 4%, respectively. Each particle is shown from two viewpoints 90° apart. (100 μm scale line for all the images.)

fall into essentially three categories: (i) compact hexagonal particles, (ii) florid particles with thin, plate-like side planes, and (iii) polycrystals. Examples of compact hexagonal crystals grown from frozen droplets are shown in Fig. 2, and examples of compact hexagonal crystals grown from seeds are shown in Fig. 3. Note the crystals grown from seeds appear considerably more pristine (transparent and apparent-defect free) than those grown from frozen droplets, although it is difficult to reproduce images of the crystals with sufficient clarity here to show all the differences evident during laboratory observations. (Further examples are posted on our website: http://www.geophys.washington.edu/Surface/Atmospheric/icephys/main.html, January 2003.) Figures 4 and 5 show examples of polycrystals and florid crystals, respectively. Note the polycrystals are quite irregular with no apparent single-crystal orientation and the polycrystals grown at higher growth rates exhibit secondary crystallites with no single apparent orientation. Florid crystals occur only at higher growth rates and have a single well defined central-crystal orientation (the central crystal is a hexagonal prismatic crystal) but with well oriented secondary thin plate-like crystallites extending from the prism facets.

We examined growth and sublimation (g/s) rates for the crystals grown from frost, frost seeds and droplets and in all cases the spherical-equivalent radius varies with time

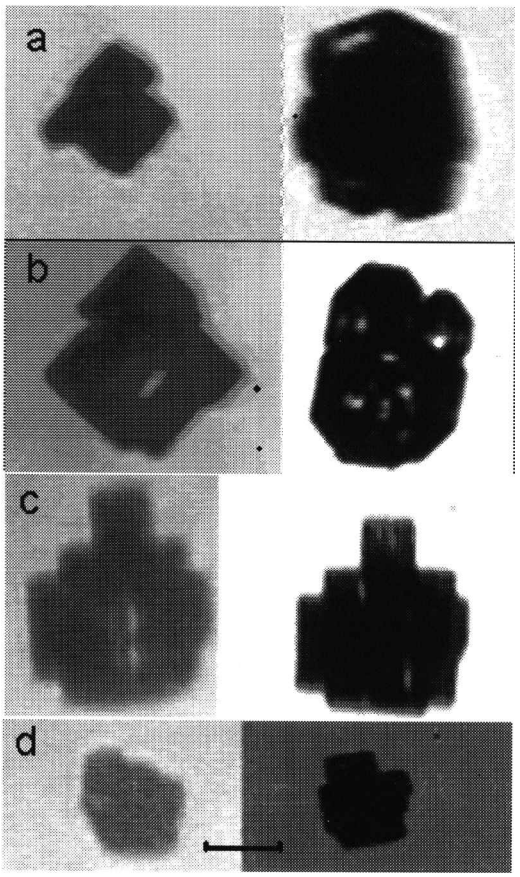

Figure 4. Examples of compact polycrystals grown from heterogeneously frozen droplets. Images of compact polycrystals grown from homogeneously frozen droplets looked quite similar. Temperatures and supersaturations for the particles shown here range from −9 to −22 °C and 2 to 13%, respectively.

as $r_{eq}(t) \propto t^{1/2}$ within our errors, independent of final morphology (hexagonal plates, hexagonal columns, florid or polycrystalline). This indicates that heat and mass diffusion (and not surface impedance) are the dominant rate-limiting processes for these particle sizes and temperatures. These g/s rate results are presented elsewhere (Swanson *et al.* 1998, 1999; Swanson *et al.*, submitted to *Rev. Sci. Inst.*).

(*a*) *Aspect ratios: Compact hexagonal crystals*

We measured the aspect ratio Γ, defined operationally as the ratio of the longest dimension in the $\hat{c}$ direction (normal to a basal facet) to that in the $\hat{a}$ direction (normal to a prism facet). We conservatively estimate the error in Γ to be ±0.2 due to our inability to measure the precise particle alignment with respect to the camera. Neither the florid particles nor the polycrystals fall easily into the categorization of crystals with hexagonal prism-like primary habits, and we omit them from our aspect-ratio study. This eliminates most of the particles grown at temperatures below about $T = -22\,^{\circ}\mathrm{C}$, which tended to be polycrystalline or at least florid at all supersaturations. Moreover, as shown in previous work (Swanson *et al.* 1999), particles starting as irregularly shaped

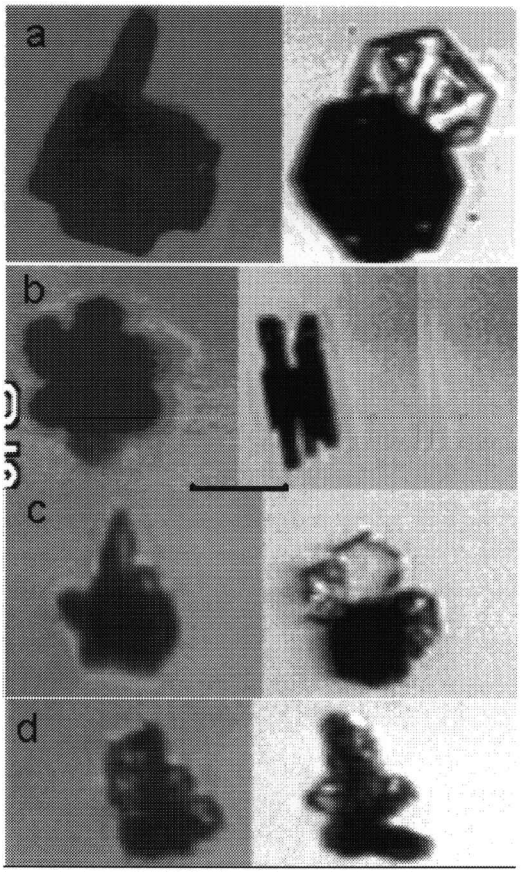

Figure 5. Examples of florid particles with side planes grown from heterogeneously frozen droplets. Temperatures and supersaturations for the particles shown here range from −14 to −27 °C and 4% to 18%, respectively. The particles shown in (a), (b), and (c) appear to be single crystals. (100 μm scale line for all the images.)

TABLE 1. SUMMARY OF OUR FINDINGS FOR BOTH DROPLET-INITIATED AND SEED-INITIATED ICE PARTICLES GROWN TO A FINAL SIZE OF 100–200 μM

Initiation	Γ	T dependence?	σ_∞ dependence?	Comments
Drops	Mixed 0.6–1.5	No for $T > -22$ °C Plates below −22 °C	More florid at higher σ_∞	Rough faces
Seeds	Mixed 0.4–8 but few with $0.8 < \Gamma < 1.2$	No	No	Very flat faces No florids

T = temperature, Γ = aspect ratio, σ_∞ = ambient supersaturation.

frost particles nearly always grew to be polycrystalline particles and, thus, were also excluded from this analysis.

The major features of our results are summarized in Table 1. The data for the particles formed from frozen droplets are shown in Fig. 6. We observe no significant temperature, vapour-excess or supersaturation dependence in primary habit of compact particles grown from droplets in the temperature range from −4 °C to −38 °C. In several cases both thick plates and short columns were observed at the same temperature and humidity conditions.

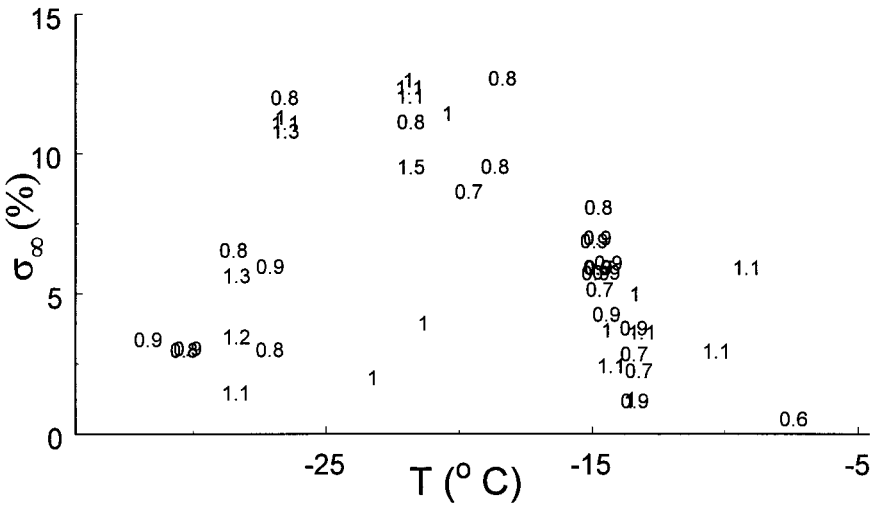

Figure 6. Ambient supersaturations σ_∞, for the final aspect ratio (Γ) of ice particles grown at various temperatures and growth rates from frozen droplets. Note: most particles grown from frozen droplets remain nearly isometric. Only compact hexagonal particles (no polycrystal or florid crystals) are included in this figure. The measurement error in Γ is estimated at ± 0.2.

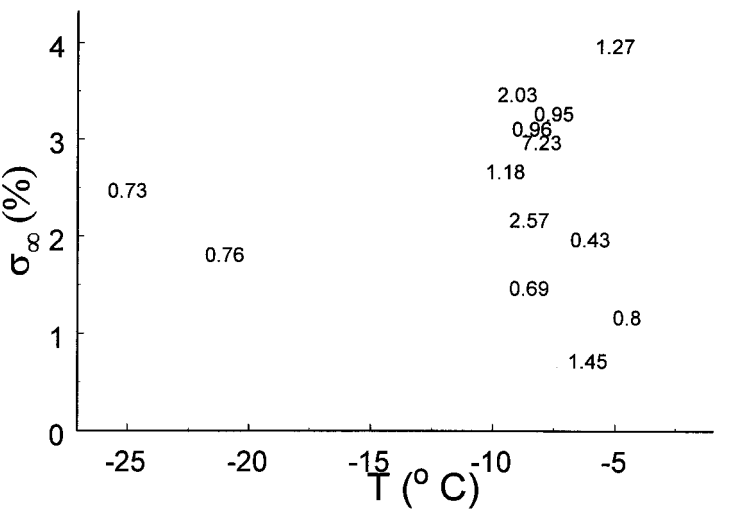

Figure 7. Ambient supersaturations σ_∞ for the final aspect ratio for ice particles grown from seed particles at low supersaturation. Note: growth under nearly identical conditions results in a wide variety of crystal aspect ratios.

Figure 7 shows the analogous data for seed-initiated ice particles. These particles (all of which started growth at sizes less than 10 μm seeds) tended to grow into hexagonal prism-like single crystals at all temperatures; polycrystalline or florid particles were seldom observed (Swanson *et al.* 1999; Swanson *et al.*, submitted to *Rev. Sci. Inst.*). These crystals had significantly sharper, flatter faces than did the particles that evolved from frozen drops, and they were more often anisometric with a wide variety of aspect ratios observed for particles grown under similar temperature and supersaturation conditions.

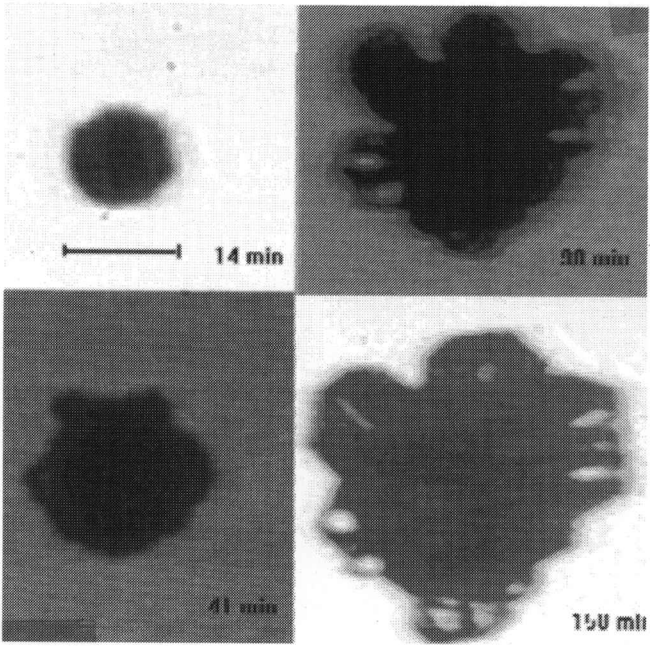

Figure 8. Growth sequence of a rosette-like homogeneously nucleated polycrystal grown at temperature $T = -30.6\,^{\circ}\mathrm{C}$ and 7.6% supersaturation. The scale in the first frame is 100 μm.

(*b*) *Florid single crystals*

A large subset of our crystals were 'florid'; i.e. they exhibited side plate-like crystals growing from part of their prism faces, with axes aligned with those of the main crystal. In most cases the thin plates were located at the crystal extremities, and we can understand the phenomenon as resulting from the non-uniform growth drive brought about by diffusion of vapour and heat to a non-spherical crystal. (In many such crystals, particularly those grown at supersaturations above 4%, ribbed structures appeared such as those shown in Figs. 5(a) and (c). These result from an additional growth instability (Frank 1982).)

Florid particles appear also in pictures from the low-supersaturation studies of Rottner and Vali (1974) although no temperature dependence is reported; it appears that the side planes are relatively perfect hexagonal prisms, and that, if the instability occurs, the side planes grow rapidly. The side planes may actually become so large they become the largest part of the particle. This would explain how the originally isometric, compact crystals that form from frozen drops turn into more anisometric particles as they grow.

We observed side planes throughout the temperature range $-38\,^{\circ}\mathrm{C}$ to $-13\,^{\circ}\mathrm{C}$, an unexpected outcome since most previous reports (e.g. Kobayashi 1961; Fukuta and Takahashi 1999) indicate a columnar primary habit below $-22\,^{\circ}\mathrm{C}$. However, other investigators (Gonda 1977; Bailey and Hallett 2000) have found plate-like habits in this range. Examples of plate-like morphologies below $-22\,^{\circ}\mathrm{C}$ in the present study are shown in Figs. 5(d) and 8. The morphology shown in Fig. 5(b), a 'capped plate', was common at about $-14\,^{\circ}\mathrm{C}$ and appeared even at moderate supersaturation. Such double-plate crystals seem to be associated with growth from frozen droplets; similar examples have been observed previously in both the laboratory and field (Veal 1954; Heymsfield

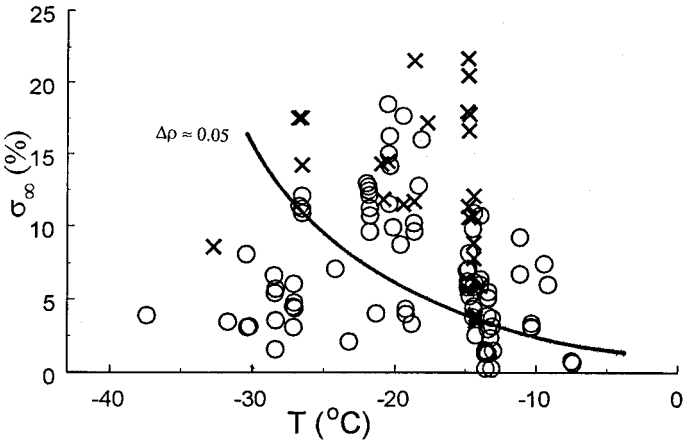

Figure 9. Plot of best-fit supersaturation (σ_∞) versus temperature for ice particles grown from frozen droplets. The symbol used indicates habit type: X for florid (has thin side planes), O for compact hexagons and compact polycrystal particles. Line is vapour excess $\Delta\rho = 0.05$ g m^{-3}. Transitional (almost florid), and rosette-type polycrystals were omitted for clarity.

1973). The particle shown in Fig. 5(b) exhibits the sector-plate morphology similar to that observed by Nakaya (1954) and others (e.g. Fukuta and Takahashi 1999), classified as P1c in the Magano and Lee scheme (Magano and Lee 1966).

Florid crystals appeared preferentially at relatively high supersaturations (above about 0.05 g m^{-3}) as is evident in Fig. 9, which shows florid and compact crystals in supersaturation–temperature space. For clarity, obvious polycrystals and transitional particles were omitted from this figure. However, the compact–florid transition is rather gradual and by no means sharp.

The gradual compact–florid transition and regions of mixed morphology that we observed are in marked contrast to those presented by Gonda and co-workers (Gonda and Koike 1982; Gonda and Yamazaki 1982; Gonda and Koike 1983), who indicated a very sharp transition from stable to unstable facets for crystals growing on a glass substrate. The sizes and supersaturations at which this transition occurs vary with size and crystal habit, but appear to be broadly similar to the transition we observed. However, these papers (Gonda and Koike 1982; Gonda and Yamazaki 1982; Gonda and Koike 1983) did not show the data explicitly and the transitions between morphological regimes were shown as infinitely sharp, where one might expect a spread of behaviour due to variations in dislocation structure and local conditions.

5. Surface structure and growth mode

As background to the discussion of our observations, we introduce the notation of Wood *et al.* (2001) to describe the surface structure of the crystals; crystals without dislocations or defects are termed D_0; those with defects on only a set (prism or basal) of facets are termed D_1, and those with defects on all facets are D_2.

Our observations suggest that the particles we grew from droplets are probably D_2, whereas those grown from frost seeds are likely to be D_1. We now give several arguments supporting this view.

(*a*) *Frozen droplets as D_2 crystals*

Our frozen-droplet particles start as molecularly rough spheres: if they were free of dislocations, one would expect a sudden change in growth rate as soon as rough areas on the initial spherical particle had developed into molecularly flat facets. This change would be most noticeable at low growth rates: if the ambient saturation σ_∞ were below the critical value for layer nucleation σ_{2D}, (Shaw and Mason 1955; Nelson and Knight 1998), this growth would switch off altogether in the absence of spiral steps or other sources of ledges. That we do not observe such behaviour (i.e. in plots like Fig. 1) is strong evidence in favour of plentiful dislocations.

Moreover, the crystals are isometric at low supersaturations (see Fig. 6). If dislocations were absent (if they were D_0 crystals) or occurred on only a subset of facets (D_1 crystals), then non-isometric habits would result at low growth rates due to the vapour-sink effect: one facet acts as a vapour sink thereby preventing growth on the other facet.

(*b*) *Frost seeds as D_1 crystals*

Seed-initiated particles grew stably (i.e. without morphological instabilities) and often anisometrically, as plates or columns, at supersaturations of only a few percent at all temperatures. The stability of the growth suggests that the ambient supersaturations were less than those giving rise to layer nucleation, which is consistent with model results (Wood *et al.* 2001) at these temperatures and ambient humidities, and the anisometric shapes suggest that in most cases growth occurred primarily on one or the other set of facets.

The fact that dissimilar crystals grow under near-identical conditions for particles grown from frozen droplets and those grown from seeds points to an inherent, formation-dependent variability in dislocation structures (Nelson 2001). It is likely that many of the particles grown from seeds were D_1 with spiral dislocations on one set of facets only, whereas, as stated above, the particles grown from frozen droplets appear to have been primarily D_2, i.e. to have dislocations on all facets.

We now focus our analysis of our observations on two questions, namely: (a) what determines the morphology of compact crystals and (b) what determines the transition to florid crystals?

(*c*) *What determines the morphology of compact crystals?*

It is clear that for the parameter ranges we have discussed, environmental temperature and humidity do not uniquely determine the overall ice-particle aspect ratio, the roughness of the surfaces (which may be important for cloud radiative properties) or the degree of polycrystallinity. The remaining factors include (i) difference in ice formation mechanism, (ii) differences in initial particle size, and (iii) differences in mass growth factors.

(i) *Initiation process.* Our results suggest that in the early growth stages the crystal aspect ratio depends to some considerable extent on the ice formation process itself, probably through dependence of dislocation/defect density on the ice initiation process. Moreover, differences in freezing temperature seem to impact subsequent particle morphology. The drops that turned into compact, single crystals were typically frozen heterogeneously at high temperatures; they froze fairly slowly as they fell from room temperature into the chamber. Particles initiated from droplets at lower temperatures probably froze at a faster rate; resulting in more polycrystalline particles. This may have been the result of multiple nucleation events resulting in an enhanced initial defect density.

The pristine transparent appearance of seed-initiated crystals indicates fewer defects present in the crystal. The initial growth direction is apparently set during initial ice-crystal initiation near the substrate and growth can proceed primarily on one facet in this limit of relatively few dislocations. Perhaps some of the variation in crystal shape reported in previous studies is caused by the use of various substrates or other non-atmospherically relevant nucleants, like silver iodide, where ice-substrate epitaxy may influence crystal shape even in a temperature-dependent manner.

(ii) *Initial particle size.* The droplets we froze were about 30–60 μm and our final particles were smaller than the non-isometric particles described in most previous experiments. Some studies have shown that aspect ratios become more extreme with increasing size (Ryan *et al.* 1976; Auer and Veal 1979), and it may be that our frozen droplets remained more isometric than those of previous studies (Hallett and Mason 1958; Kobayashi 1961; Fukuta and Takahashi 1999) because we examined them when they were still small ($<$200 μm). Crystals grown from large frozen droplets may develop complex morphologies at lower supersaturations than those grown from small droplets. There are several reasons for this. First, the larger the droplet the more likely it is to freeze as a set of polycrystals (Pitter and Pruppacher 1973; Pruppacher and Klett 1997). Second, the larger the original droplet the more likely it is to have dislocations near its surface. These tend to maintain a rather uniform vapour sink around the entire particle and facilitate the development of randomly oriented surface crystals yet do not permit rapid growth of any particular face.

However, given the fact that the particles grown from frost seeds were also small, size alone cannot be a dominant reason for the isometric habits of the particles we grew from frozen drops.

(iii) *Mass growth factor.* From previously published reports, it appears that non-isometric habits develop only after the crystal masses reach nearly 1000 times the masses of the original drops. In several cases this means the habit develops after the linear dimension of the crystals reaches approximately 100 μm. That is, the habits are not in evidence until the spherical-equivalent radius of the ice particle reaches about 10 times the size of the initial droplet. Our frozen drops were followed as their masses grew by a factor of not more than 10. A natural question to ask is whether their isometric habits result from similar growth rates on *c* and *a* faces, or whether they can be simply explained by the limited mass increase over that of the initial sphere shape? In evolving from a sphere to an isometric hexagon of the same diameter, the particle mass increases by a factor of about 1.65. A particle that subsequently grows only on the *a* faces will develop an aspect ratio of about 0.4 after a tenfold increase in mass; one growing only on the *c* faces will reach an aspect ratio of about 6. The average mass gain for the particles shown in Fig. 6 was 11.2 ± 4.5, with a minimum of 5.1. Even this smallest mass gain could lead to aspect ratios of 0.55 or 3.1 for growth restricted to either the prism or basal faces. This clearly is not the case for our crystals and the fact that the observed aspect ratios are so close to unity demonstrates that both *a* and *c* facets grew in all cases.

The final size of seed-initiated particles was similar to those initiated from droplets (100–200 μm). Yet in our earlier experiments on ice particles grown from seeds (Fig. 7) the masses of the ice particles grew by factors of more than 10^2. Thus it may be that small differences in the growth rates of the two faces were able to manifest themselves as more anisometric habits partly because each crystal face increased its area so greatly.

6. Experimental results: Compact–florid transition

(*a*) *Definition of floridity*

We quantified the 'floridity' of our crystals by means of an image analysis algorithm using measurements of the particle's perimeter p and projected area A to determine a particle irregularity index I. Analysis of this parameter for single crystals shows that, even in the lowest temperature range, where polycrystals dominate, I increases with supersaturation, even though the range of supersaturation corresponds to a much smaller growth rate at low temperature.

It is likely that similar facet instabilities take place in polycrystals, (at low growth rates polycrystals remain relatively compact while higher growth rates tend to result in particles with side plates with random orientations) although the crystal complexity makes such features hard to quantify visually. Figure 8 shows the evolution of an apparent polycrystal from a homogeneously frozen droplet. The initial evolution resulted in a particle that resembled a single hexagon, seen after 14 minutes of growth. This particle later sprouted plate-like protrusions whose major axes do not appear to fit into a single-crystal framework. Variously shaped polycrystals occur frequently under low-temperature growth conditions ($T < -25\,^{\circ}\mathrm{C}$) particularly from homogeneously frozen liquid droplets where the freezing temperature $T_{\mathrm{freezing}} < -35\,^{\circ}\mathrm{C}$.

In the following discussion, we are not concerned with distinctions among florid crystals but rather the transition from stable (compact) to unstable growth. For this purpose we use a rough visual criterion to distinguish 'florid' from 'compact' crystals.

(*b*) *Dependence of transition on environmental parameters*

First we present the distribution of compact and florid crystals as functions of temperature and environmental supersaturation. Figure 9 shows that there is a region of supersaturation–temperature space in which both compact and florid crystals (defined visually) occur. There appears to be an upper transition above which only florid morphologies are found, and possibly a lower transition below which only compact morphologies develop. We now use these observed transitions, together with a crystal growth model, to infer the surface parameters determining crystal evolution.

(*c*) *Growth parameters inferred from observed transitions*

From the data shown in Fig. 9, only the particles initiated as heterogeneous frozen droplets—predominantly single-crystal particles—lend themselves to facet-stability analysis because facet instabilities are hard to identify optically in polycrystals. The facet instability we observed took place only on the prism faces, which means that the basal-face instability (which manifests itself as hollowing) occurs at higher supersaturation than that on the prism face. We can use the results of the Wood *et al.* (2001) growth model to deduce $\sigma_{2\mathrm{D}}(T)$ for the prism face from the observed morphological transitions.

In order to proceed further, we consider the location of dislocations on D_2 crystals. D_2 crystals with defects in the middle of each facet are denoted $D_{2\mathrm{m}}$, whereas those with defects at facet edges are $D_{2\mathrm{e}}$. Yokoyama (Yokoyama and Kuroda 1990; Yokoyama 1993) has discussed the case in which spiral dislocations are located near the crystal corners, which can lead to facet instability. $D_{2\mathrm{m}}$ crystals are stable at relatively high supersaturation because the vapour-sink effect of spiral growth inhibits layer nucleation at the corners. Those with dislocations near the edges ($D_{2\mathrm{e}}$) are susceptible to facet instability; i.e. spiral growth near the edges leads to unstable facets at low growth rates—a point we will show in the appendix. Below the compact–florid transition for $D_{2\mathrm{m}}$ crystals, $D_{2\mathrm{m}}$ crystals grow compact, while $D_{2\mathrm{e}}$ crystals grow with a florid morphology.

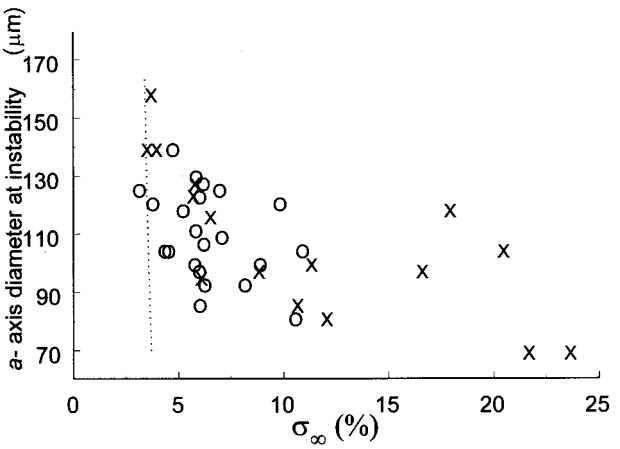

Figure 10. Size (a-axis diameter) and ambient supersaturation (σ_∞) dependence for onset of facet instability at temperature $T = -14.5 \pm 0.5$ °C. Shown are florid (X) and compact (O) particles grown from 40 μm frozen droplets. The dotted line is the onset of facet instability predicted by Eq. (A.8) for D_0 crystals with $n = 10$ and $\sigma_{2D} = 2.4\%$ (Table 2). The presence of compact particles at higher supersaturations than this line is consistent with our hypothesis that the crystals are primarily D_{2m} (spiral dislocations outcropping near the middle of facets). The scatter in the data can be accounted for by invoking a variety of dislocation structures (see text).

We, therefore, assume that the supersaturation above which we observe all crystals to undergo prism facet instability (the 'upper transition') is the lower limit for the instability for D_{2m} crystals. Wood *et al.* (2001) show that for D_{2m} crystals at the onset of facet instability the ratio $\sigma_\infty/\sigma_{2D}$ is approximately 4.2 for 100 μm scale ice crystals, with very little dependence on crystal size. Using this result, we deduce lower limits for $\sigma_{2D}(T)$ from the upper transition at -15 °C, -20 °C, and -25 °C. The results are shown in Table 2. The values obtained lie between those reported by Nelson and Knight (1998) and Shaw and Mason (1955). We account for the region of mixed morphology in Fig. 9 by proposing that dislocations outcrop at different points on individual crystals. Those with dislocations near the middle of facets are the least prone to facet instability. Thus the results for $\sigma_{2D}(T)$ given by the upper transition are best understood as lower limits.

(*d*) *Dependence of transition on particle size*

The compact–florid transition data at -15 °C are shown in Fig. 10 and those at -25 to -30 °C are shown in Fig. 11 along with model predictions for ideal dislocation-free isometric crystals with $n = 10$ in Eq. (A.8) using best-guess σ_{2D} values from Table 2.

The appendix contains an analytic model for the size dependence of the ambient supersaturation threshold σ_∞ for onset of facet instability. The results are shown in Fig. 12, where σ_X is a scaling parameter that depends on the growth mechanism assumed; the parameter n varies from $n = 1$ for dislocation growth to higher values for layer nucleation (see appendix). Each curve on the figure separates the region of stable growth from that of unstable growth for the assumed values of n and σ_X.

(*e*) *Comparison of observations and model*

Comparison of the data in Figs. 10 and 11 with the theoretical facet instability curve in Fig. 12 allows us to constrain the growth mechanism that drives the observed florid morphologies. If the dominant mechanism were spiral growth at the corners (Fig. 12,

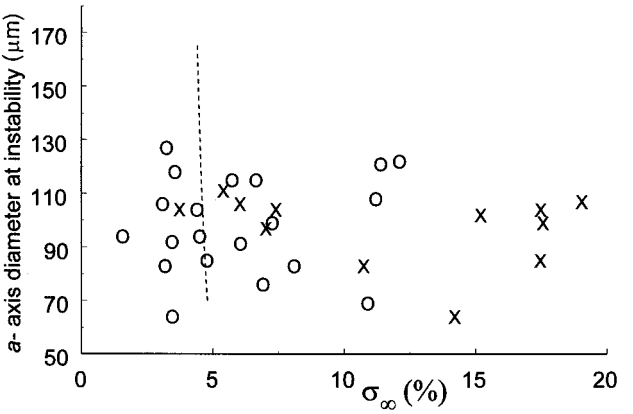

Figure 11. Size (a-axis diameter) and ambient supersaturation (σ_∞) dependence for onset of facet instability at temperature $T = -27.5 \pm 2.5\,^{\circ}\mathrm{C}$. Shown are florid (X) and compact (O) particles grown from 40 μm frozen droplets. The dotted line is the onset of facet instability predicted by Eq. (A.8) for D_0 crystals with $n = 10$ and $\sigma_{2D} = 2.4\%$ (Table 2).

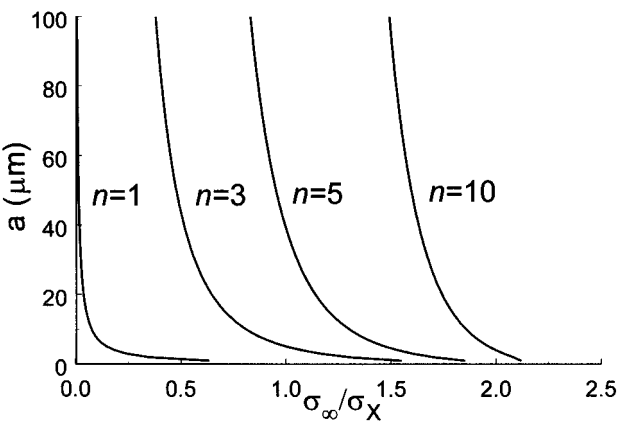

Figure 12. Size (a-axis diameter) and ambient supersaturation (σ_∞) dependence of facet instability for growth initiated at the crystal corners, given by Eq. (A.8), for different values of n in Eq. (A.6): $n = 1$ corresponds to growth by spiral steps (in which case σ_X denotes σ_1), while higher values of n represent layer nucleation (σ_X denotes σ_{2D}). The area to the left of each curve represents stable growth, and to the right the prism facets are unstable.

$n = 1$) then, stability for a 50 μm wide crystal at supersaturation $\sigma_\infty = 10\%$ would require $\sigma_X = \sigma_1 \approx 500\%$. This magnitude is inconsistent with other measurements; for example, Gonda *et al.* (1994) gave $\sigma_1 = 1.1\%$ at $-15.5\,^{\circ}\mathrm{C}$ and 0.98% at $-28.5\,^{\circ}\mathrm{C}$. This inconsistency suggests that most of the crystals we observed were not growing by spiral dislocations near the corners. In contrast, the curve $n = 10$ in Fig. 12 shows that instability on similar crystals growing by layer nucleation at the crystal corners requires σ_{2D} values in the (much more plausible) range of a few percent. Another possibility, which requires numerical calculation, is that the crystals are D_{2m} and that the instability results from layer nucleation at the corners competing with spiral growth at face centres. In this case stability occurs at higher values of $\sigma_\infty/\sigma_{2D}$. This is the growth scenario used to predict the values of $\sigma_{2D}(T)$ in Table 2.

TABLE 2. AMBIENT SUPERSATURATIONS σ_∞ FOR UPPER TRANSITIONS IN MORPHOLOGY EVIDENT IN FIG. 9 (SEE TEXT FOR EXPLANATION), AND INFERRED CRITICAL SUPERSATURATIONS FOR LAYER NUCLEATION σ_{2D} ON PRISM FACES

T	$-15\,^\circ$C	$-20\,^\circ$C	$-25\,^\circ$C
σ_∞ (upper transition)	11%	20%	14%
σ_{2D} (upper transition, $D2_m$)	$\geq$2.4%	$\geq$4.4%	$\geq$3.1%
σ_{2D} (Nelson and Knight 1998)	0.6%	–	–
σ_{2D} (Shaw and Mason 1955)	$\geqslant$6%	–	$\geqslant$10%

The values obtained lie between those reported by Nelson and Knight (1998) and Shaw and Mason (1955).

Figures 10 and 11 show that for larger particles there is a weak tendency for florid particles to appear at lower supersaturations. However, the scatter in the data is large. It appears that size variations alone cannot explain the mix of morphologies, as we noted in section 5. Rather, the mix can be explained only by invoking a variety of dislocation distributions on the surface of the particles: those with dislocations near the edges undergo facet instability at low supersaturations.

The analysis presented here has shown that growth due to spiral dislocations at the crystal corners leads to facet instability at low supersaturations. Perhaps the reason that the theoretical work of Yokoyama (Yokoyama and Kuroda 1990; Yokoyama 1993) found the facets to be stable at moderate supersaturations is that their model was only two dimensional.

7. DISCUSSION AND ATMOSPHERIC IMPLICATIONS

In this study, we have followed the evolution of ice particles in air from frozen drops and frost seeds to faceted crystals at relatively low supersaturations. Our results are summarized in Table 1. We find that particle morphology in the initial stages of growth depends to some considerable degree on the ice initiation process (and perhaps the initial ice-particle size).

Throughout the temperature range -25 to $-4\,^\circ$C, we found, as have others, that the compact single crystals formed from frozen drops were quite isometric at vapour excesses of less than about $\Delta\rho = 0.05$ g m^{-3}. Our crystals were somewhat more isometric than those in the literature, but the range of published aspect ratios for low growth rates, like the range we found, is fairly broad. At temperatures below about $-22\,^\circ$C drops froze mainly as polycrystals, as did all particles grown from frost. In general it appears that at slow growth rates ice-particle morphology is not unique to particular temperature and humidity conditions and seems to also depend on the ice initiation process. We suspect that the determining factor is the concentration of crystalline defects in the initial particle. We observed that an instability which occurs on the prism facets occurred on some frozen droplets at a vapour excess $\Delta\rho \approx 0.05$ g m^{-3}, well below the transition to dendrites given by Kobayashi (1961).

From our observations we infer that ice-particle growth was mediated by dislocations throughout the range of parameters in our study. Particles grown from small seeds often appear to be D_1, with few defects at the surface. At environmental supersaturations too low to allow layer nucleation on any of the facets, the faces with dislocations grow and the others do not, creating anisometric plate-like and columnar crystals at the same environmental conditions. We suggest that many of the frozen drops we observed going through facet instability were crystals that had spiral dislocations near their corners.

(*a*) *Atmospheric implications*

Our observations suggest that traditional ice-particle habit diagrams, showing the observed aspect ratios of compact ice crystals as functions of growth conditions are not sufficient to explain important features of small ice crystals in fully glaciated stratiform clouds. Our results may explain the finding of rather isometric, but irregular, florid crystals in Arctic clouds (Korolev and Isaac 1999), and the finding (Walden *et al.* 2003) of particles of extreme columnar and plate-like habits near the south pole in Antarctic temperatures ($-40\,^{\circ}$C and below), where the initial particles may be small and the critical supersaturations for layer nucleation, σ_{2D}, appear to be relatively high (Nelson 2001; Wood *et al.* 2001). Moreover, anecdotal evidence of the abundance of pristine crystals in the 'Hallett–Mossop' zone of cumuliform clouds (Rangno and Hobbs 2001) may be due to the fact that these crystals are formed on the tiny fragments of ice created by shattering during drop impact on soft hail.

The radiative importance of fully glaciated clouds requires more careful examination of the evolution and scattering properties of the small, compact crystals within the clouds. Our finding that not only overall particle shape but also facet smoothness and small-scale surface roughness are related to ice initiation processes may, if confirmed by further studies, have serious implications for radiative transfer in glaciated clouds, particularly at high latitudes.

It would be desirable to extend the temperature range of the kinds of measurements we have made (which should be possible in our EDB) down to $-60\,^{\circ}$C and to be able to increase environmental supersaturations to water saturation. Our observations appear to indicate that polycrystals dominate at temperatures below $-30\,^{\circ}$C, which is not unexpected, but also that isometric or plate-like habits dominate throughout the low-growth-rate domain, a finding which we plan to revisit and extend to lower temperatures by further experiments in our chamber.

Acknowledgements

We thank Leo Shen and Andy Mason at the Hewlett Packard Corporation for supplying the inkjet cartridges and Wayne Palmiter at York International for providing samples of SNOMAX. We also thank Jim Davis and Mary Laucks for helpful experimental suggestions, Steve Wood for valuable model results, and Robert Synovec, Wes Quigley and Song Gao for help with the chemical analysis. Support for this research came from the Leonard X. Bosack and Bette M. Kruger Charitable Foundation, and National Science Foundation grants ATM-9528049,9704156 and ATM-9906538.

Appendix

Model for facet-instability onset

In this section we develop a closed-form expression for the critical ambient supersaturation, denoted $\sigma_{\infty}^{a}(\mathrm{cr})$, for the onset of the facet instability of a relatively isometric crystal with typical dimension 'a' in the case of the ledges being generated only at the crystal corners. We then compare the results with values extracted from our data. The basic idea is that with increasing σ_{∞} the step propagation at the surface eventually cannot keep up with the diffusive flux and the growth becomes unstable.

According to standard theory (Burton *et al.* 1951; Nelson 2001) the net flux of molecules from the vapour to a point $\mathbf{x}$ on the flat surface of a growing crystal is proportional to the product of $\sigma_s(\mathbf{x})$, the surface supersaturation at that point, and

$\alpha\{\sigma_s(\mathbf{x})\}$, the condensation coefficient there. That is,

$$J(\mathbf{x})\{(\mathrm{m}^2\ \mathrm{s})^{-1}\} \propto \alpha\{\sigma_s(\mathbf{x})\}\sigma_s(\mathbf{x}). \tag{A.1}$$

The flux given by Eq. (A.1) must be equal to the flux of molecules diffusing toward the crystal from the environment, which is a function of the ambient supersaturation, diffusivity and the size and shape of the crystal. Previous authors (Nelson 1994; Nelson and Baker 1996; Wood *et al.* 2001) have shown that, on the surface of a hexagonal crystal during faceted growth, the mixing-ratio field can be expressed as a linear superposition of functions $Q(\boldsymbol{\zeta})$ (where $\boldsymbol{\zeta} = (\mathbf{x}/a)$ is the displacement scaled by the crystal dimension a) that satisfy Laplace's equation in the exterior and have uniform, unit-normal gradient at the prism or basal faces:

$$\nabla_\perp\, Q(\boldsymbol{\zeta}) = 1 \qquad \text{at prism-face boundaries} \tag{A.2}$$

$$\nabla_\perp\, Q(\boldsymbol{\zeta}) = 0 \qquad \text{at basal-face boundaries.} \tag{A.3}$$

A similar function can be defined for growth on the basal faces, but we will not consider that here, since the instability we observed occurred on the prism faces. The value of $Q(\boldsymbol{\zeta})$ varies over the surface of the crystal: it is lowest at the corners (value Q_c), and highest in the middle of facets, where its value is Q_m. For a given ambient supersaturation σ_∞, assuming the steps are generated at the corners, we can match the flux through the vapour to the surface flux at the corner (see Eq. (A.1)) to find

$$\frac{\sigma_\infty - \sigma_c}{a\,Q_c} = \frac{\alpha(\sigma_c)\sigma_c}{\lambda}, \tag{A.4}$$

where λ is the mean free path of vapour-phase water molecules.

For stable faceted growth, the flux (Eq. (A.1)), is uniform over the entire facet. (Here we assume the crystal, and in particular its surface, is isothermal.) Equating $\alpha\sigma$ at the corner and at the middle of the prism facets, we find from Eqs. (A.1) and (A.4) that the condensation coefficient at the middle of the face is

$$\alpha_m = \frac{\sigma_\infty - \sigma_c}{(a/\lambda)\{Q_m\sigma_c - (Q_m - Q_c)\sigma_\infty\}}. \tag{A.5}$$

$\alpha_m > 1$ is unphysical and indicates that the growth at the centre can not match that at the corners. Note that Q_m and Q_c are constants set by the geometry, and that $Q_m > Q_c$. The first thing to notice about Eq. (A.5) is that $0 < \alpha_m < 1$ requires that $\sigma_c > \{(Q_m - Q_c)/Q_m\}\sigma_\infty$. Wood *et al.* (2001) have evaluated the basis functions for growing hexagons of various aspect ratios. For an isometric hexagon growing on the prism faces, $Q_m = 1.18$ and $Q_c = 0.74$, implying that faceted growth initiated at the crystal corners is impossible unless $\sigma_c > 0.37 \times \sigma_\infty$. In other words, such corner-driven growth cannot preserve facets unless the surface kinetics maintain the surface supersaturation at a significant fraction of the ambient value.

The condensation coefficient

To proceed, we need the dependence of the condensation coefficient α on surface supersaturation σ_s. The flux is uniform on a flat facet and is equal to its value at the ledge sources. We denote the values of parameters measured at ledge sources by asterisks. The function $\alpha^*(\sigma_s^*)$ thus determines the flux everywhere on the facet. If spiral dislocations provide the ledges, then α^* increases steadily with σ_s^*, and is greater than zero as long as $\sigma_s^* > 0$. For crystals growing by layer nucleation, $\alpha^*(\sigma_s^*)$ is a highly nonlinear function of σ_s^*.

The algebraic form of $\alpha^*(\sigma_s^*)$ used by different authors varies (Burton *et al.* 1951; Kuroda and Lacmann 1982; Nelson and Baker 1996; Nelson and Knight 1998), and the microscopic surface parameters that determine α^* are poorly known for ice. Therefore, we adopt a simple, generic form for α^* introduced by Nelson and Baker (1996) namely,

$$\alpha^* = \left(\frac{\sigma^*}{\sigma_X}\right)^n \tanh\left\{\left(\frac{\sigma_X}{\sigma^*}\right)^n\right\}, \tag{A.6}$$

where $n = 1$ describes the behaviour if outcropping of spiral dislocations provides the ledges and $n \gg 1$ produces an $\alpha^*(\sigma_s)$ function that is zero for $\sigma_s^* \leqslant \sigma_X$ and then rises steeply to 1, thus capturing the major characteristics of layer nucleation. The parameter σ_X incorporates the microscopic surface parameters and temperature dependence of the condensation coefficient; for spiral dislocations σ_X is often denoted σ_1, and for layer nucleation $\sigma_X \equiv \sigma_{2D}$, the threshold surface supersaturation for nucleation. In principle σ_X can be computed from these microscopic surface parameters; using an idealized pillbox geometry for the critical nucleus and the best available values of surface free energy (Hobbs 1974) yields $\sigma_{2D} \approx 25\%$ for $T = -10\,^\circ$C. Given the uncertainty in the parameters in this calculation, however, the values of σ_X must be inferred from experiment.

For relatively low surface supersaturations, and particles much larger than the vapour mean free path, the flux-matching condition Eq. (A.4) together with the surface kinetic condition Eq. (A.6) and Eq. (A.5) give the limit of faceted growth as a size-dependent condition on σ_∞ such that $\alpha_m = 1$.

$$\sigma_s^* = \sigma_c = \left(\frac{\lambda \sigma_X^n \sigma_\infty}{a Q_c}\right)^{\frac{1}{n+1}}, \tag{A.7}$$

and

$$\sigma_\infty^a(\mathrm{cr}) = \sigma_X \left(\frac{\lambda}{a Q_c}\right)^{1/n} \left(\frac{1 + Q_m a/\lambda}{1 + (Q_m - Q_c)a/\lambda}\right)^{\frac{n+1}{n}} \tag{A.8}$$

as the limiting condition for facet stability in this slow-growth approximation.

In Fig. 12, we show the limiting curves for stable growth calculated from Eq. (A.8) for different values of n. (Note how the limiting supersaturation (scaled by the surface kinetic parameter $\sigma_X \equiv \sigma_1$ or σ_{2D}) increases and sharpens $\alpha^*(\sigma_s^*)$ with increasing n (J. Nelson, personal communication).) The case $n = 10$ agrees quite well with Fig. 13 of Wood *et al.* (2001) for isometric D_0 crystals. (We note, however, that the analysis has not addressed the case in which there are two competing growth mechanisms: growth by spiral dislocations at the middle of facets and growth by layer nucleation at the corners. For this case, the stability curves are displaced to the right toward larger values of the supersaturation ratio.) A striking feature of Fig. 12 is that growth due to spiral dislocation at the corners ($n = 1$) is unable to sustain facets except at very low supersaturations.

References

Arnott, W. P., Dong, Y. Y. and Hallett, J. 1994 Role of small ice crystals in radiative properties of cirrus: A case study, FIRE II, November 22, 1991. *J. Geophys. Res.*, **99,** 1371–1381

Auer, A. H. and Veal, D. H. 1979 The dimensions of ice crystals in natural clouds. *J. Atmos. Sci.*, **27,** 919–926

Bailey, M. P. and Hallett, J. 2000 'Nucleation, growth, and habit distribution of cirrus type crystals under controlled laboratory conditions'. Pp. 629–632 in proceedings of the 13th international conference on clouds and precipitation

Bartlett, J. T., van de Heuval, A. P. and Mason, B. J. 1963 The growth of ice crystals in an electric field. *J. Appl. Math. Phys.*, **14,** 599–610

Burton, W. K., Cabrera, N. and Frank, F. C. 1951 The growth of crystals and the equilibrium structure of their surface. *Philos. Trans. R. Soc. London A*, **243,** 299–358

Chen, J.-P. and Lamb, D. 1999 Simulation of cloud microphysical and chemical processes using a multicomponent framework. II. Microphysical evolution of a wintertime orographic cloud. *J. Atmos. Sci.*, **56,** 2293–3120

Chernov, A. A. and Trusov, L. I. 1969 Electrostatic effects in the formation of nuclei (seeds) at a surface. *Soviet Phys. Crystallography*, **14,** 172–178

Colbeck, S. C. 1983 Ice crystal morphology and growth rates at low supersaturations and high temperatures. *J. Appl. Phys.*, **54,** 2677–2682

Davis, E. J., Buehler, M. F. and Ward, T. L. 1990 The double-ring electrodynamic balance for microparticle characterization. *Rev. Sci. Instrum.*, **61,** 1281–1288

DeMott, P. J., Rogers, D. C., Kreidenweis, S. M., Yalei-Chen, Twohy, C. H., Baumgardner, D., Heymsfield, A. J. and Chan, K. R. 1998 The role of heterogeneous freezing nucleation in upper tropospheric clouds. Inferences from SUCCESS. *Geophys. Res. Lett.*, **25,** 1387–1390

Evans, L. 1973 The growth and fragmentation of ice crystals in an electric field. *J. Atmos. Sci.*, **30,** 1657–1664

Field, P. R., Cotton, R. J., Noone, K., Glant, P., Kaye, P. H., Hirst, E., Greenaway, R. S., Jost, C., Gabriel, R., Reiner, T., Andreae, M., Saunders, C. P. R., Archer, A., Choularton, T., Smith, M., Brooks, B., Hoell, C., Bandy, B., Johnson, D. and Heymsfield, A. 2001 Ice nucleation in orographic wave clouds: Measurements made during INTACC. *Q. J. R. Meteorol. Soc.*, **127,** 1493–1512

Frank, F. C. 1982 Snow crystals. *Contemp. Phys.*, **23,** 3–22

Fukuta, N. and Takahashi, T. 1999 Growth of atmospheric ice crystals: A summary of findings in vertical supercooled cloud tunnel studies. *J. Atmos. Sci.*, **56,** 1963–1979

Gold, L.W. and Power, B. A. 1971 Observations of ice crystal by droplets freezing in natural clouds. *J. Atmos. Sci.*, **28,** 285–290

Gonda, T. 1977 Growth of small ice crystals in gases of high and low pressures at −30 and −44 °C. *J. Meteorol. Soc. Jpn*, **55,** 142–146

Gonda, T. and Koike, T. 1982 Growth rates and growth rates of ice crystals grown from the vapour phase. *J. Crystal Growth*, **56,** 259–264

1983 Growth mechanisms of single ice crystals at a low temperature and their morphological stability. *J. Crystal Growth*, **65,** 36–42

Gonda, T. and Yamazaki, T. 1982 Morphological stability of polyhedral ice crystals growing from the vapor phase. *J. Crystal Growth*, **60,** 259–263

Gonda, T., Matsuura, Y. and Sei, T. 1994 In situ observation of vapor-grown ice crystals by laser two-beam interferometry. *J. Crystal Growth*, **142,** 171–176

Hallett, J. and Mason, B. J. 1958 The influence of temperature and supersaturation on the habit of ice crystals grown from the vapour. *Proc. R. Soc. London*, **247,** 440–453

Heymsfield, A. 1973 Laboratory and field observations of the growth of columnar and plate crystals from frozen droplets. *J. Atmos. Sci.*, **30,** 1650–1656

Hobbs, P. V. 1974 *Ice Physics.* Clarendon Press, Oxford

IPCC 2001 *Climate change 2001: Third assessment report of the Intergovernmental Panel on Climate Change (IPCC).* Cambridge University Press, Cambridge

Keller, K. W., McKnight, C. V. and Hallett, J. 1980 Growth of ice discs from the vapor and the mechanism of habit change of ice crystals. *J. Crystal Growth*, **49,** 458–464

Khvorostyanov, V. and Curry, J.	2000	A new theory of heterogeneous ice nucleation for application in cloud and climate models. *Geophys. Res. Lett.*, **27,** 4081–4084
Kobayashi, T.	1961	The growth of snow crystals at low supersaturations. *Philos. Mag.*, **6,** 1363–1370
Korolev, A. V. and Isaac, G. A.	1999	Ice particle habits in arctic clouds. *Geophys. Res. Lett.*, **26,** 1299–1302
Korolev, A. V., Isaac, G. A. and Hallett, J.	2000	Ice particle habits in stratiform clouds. *Q. J. R. Meteorol. Soc.*, **126,** 2873–2902
Kuroda, T. and Lacmann, R.	1982	Growth kinetics of ice from the vapour phase and its growth forms. *J. Crystal Growth*, **56,** 189–205
Lawson, R. P., Heymsfield, A. J., Aulenbach, S. M. and Jensen, T. L.	1998	Shapes, sizes, and light-scattering properties of ice crystals in cirrus and a persistent contrail during SUCCESS. *Geophys. Res. Lett.*, **25,** 1331–1334
Liao, J. C. and Ng, K. C.	1990	The effect of ice nucleators on snow making and spray freezing. *Ind. Eng. Chem. Res.*, **29,** 361–366
Libbrecht, K. G. and Tanusheva, V. M.	1998	Electrically induced morphological instabilities in free dendrite growth. *Phys. Rev. Lett.*, **81,** 176–179
McFarquhar, G. M. and Heymsfield, A. J.	1996	Microphysical characteristics of three anvils sampled during the central equatorial pacific experiment. *J. Atmos. Sci.*, **53,** 2401–2423
McKnight, C. V. and Hallett, J.	1978	X-ray topographic studies of dislocations in vapor-grown ice crystals. *J. Glaciol.*, **21,** 397–407
Magano, C. and Lee, C. W.	1966	Meteorological classification of natural snow crystal. *J. Fac. Sci. Hokkaido*, **2,** 321–335
Matrosov, S. Y. and Heymsfield, A. J.	2000	Use of Doppler radar to assess ice cloud particle fall velocity–size relations for remote sensing and climate studies. *J. Geophys. Res.*, **105,** 22427–22436
Nakaya, U.	1954	*Snow crystals, natural and artificial*. Harvard University Press, Cambridge, MA, USA
Nelson, J.	1994	'A theoretical study of ice crystal growth in the atmosphere'. PhD thesis, University of Washington
	2001	Growth mechanisms to explain the primary and secondary habits of snow crystals. *Phil. Mag.*, **81,** 2337–2373
Nelson, J. and Baker, M. B.	1996	A new theoretical framework for studies of vapor growth and sublimation of small ice crystals in the atmosphere. *J. Geophys. Res.*, **101,** 7033–7047
Nelson, J. and Knight, C. A.	1998	Snow crystal habit changes explained by layer nucleation. *J. Atmos. Sci.*, **55,** 1452–1465
Ono, A.	1970	Growth mode of ice crystals in natural clouds. *J. Atmos. Sci.*, **27,** 649–658
Ovtchinnikov, M. and Kogan, Y.	2000	An investigation of ice production mechanisms in small cumuliform clouds using a 3-D model with explicit microphysics. I: Model description. *J. Atmos. Sci.*, **57,** 2989–3003
Pitter, R. L. and Pruppacher, H. R.	1973	A wind tunnel investigation of freezing of small water drops falling at terminal velocity in air. *Q. J. R. Meteorol. Soc.*, **99,** 540–550
Pruppacher, H. R. and Klett, J. D.	1997	*Microphysics of clouds and precipitation*. Reidel, Dordrecht
Rangno, A. and Hobbs, P. V.	2001	Ice particles in stratiform clouds in the Arctic and possible mechanisms for the production of high ice concentrations. *J. Geophys. Res.*, **106,** 15065–15075
Rottner, D. and Vali, G.	1974	Snow crystal habit at small excesses of vapor density over ice saturation. *J. Atmos. Sci.*, **31,** 560–569
Ryan, B. F., Wishart, E. R. and Shaw, D. E.	1976	Growth rates and densities of ice crystals between −3 °C and −21 °C. *J. Atmos. Sci.*, **33,** 842–851
Sei, T. and Gonda, T.	1989	The growth mechanism and the habit change of ice crystals growing from the vapor phase. *J. Crystal Growth*, **94,** 697–707
Shaw, D. and Mason, B. J.	1955	The growth of ice crystals from the vapour. *Philos. Mag.*, **46,** 249–262
Shupe, M. D., Uttal, T., Matrosov, S. Y. and Frisch, A. S.	2001	Cloud water contents and hydrometeor sizes during the FIRE Arctic Clouds Experiment. *J. Geophys. Res.*, **106,** 15015–15028
Stephens, G. L., Tsay, S. C., Stackhouse, P. W. and Flatau, P. J.	1990	The relevance of the microphysical and radiative properties of cirrus clouds to climate and climate feedback. *J. Atmos. Sci.*, **47,** 1742–1753

Swanson, B. D., Bacon, N. J., Davis, E. J. and Baker, M. B. 1998 'Levitated ice crystals: Laboratory measurements of ice particle breakup and growth/sublimation rates'. Pp. 429–430 in proceedings of the AMS conference on cloud physics, 17–21 August 1998, Everett, WA, USA

1999 Electrodynamic trapping and manipulation of ice crystals. *Q. J. R. Meteorol. Soc.*, **125,** 1039–1058

Takahashi, T. and Fukuta, N. 1988 Supercooled cloud tunnel studies on the growth of snow crystals between −4 and −20 °C. *J. Meteorol. Soc. Jpn*, **66,** 841–855

Takahashi, T., Endoh, T. and Wakahama, G. 1991 Vapor diffusional growth of free-falling snow crystals between −3 and −23 °C. *J. Meteorol. Soc. Jpn*, **69,** 15–30

Vali, G., Christensen, M., Fresh, R. W., Galyan, E. L., Maki, L. R. and Schnell, R. C. 1976 Biogenic ice nuclei. Part ii: Bacterial sources. *J. Atmos. Sci.*, **33,** 1565–1570

Veal, A. H. 1954 Dependence of the form of natural snow crystals on meteorological conditions. *J. Meteorol.*, **11,** 35–42

Vogelmann, A. M. and Ackerman, T. P. 1995 Relating cirrus cloud properties to observed fluxes: A critical assessment. *J. Atmos. Sci.*, **52,** 4285–4301

Walden, V. P., Warren, S. G. and Tuttle, E. 2003 Atmospheric ice crystals over the Antarctic Plateau in winter. *J. Appl. Meteorol.*, in press

Welch, J. F. and Speidel, H. K. 1989 Visualization of potential bacterial ice nucleation sites. *Cryo. Lett.*, **10,** 309–314

Wood, S. E., Baker, M. B. and Calhoun, D. 2001 New model for the vapor growth of hexagonal ice crystals in the atmosphere. *J. Geophys. Res.*, **106,** 4845–4870

Wood, S. E., Baker, M. B. and Swanson, B. D. 2002 New instrument for studies of homogeneous and heterogeneous ice nucleation in free-falling supercooled water droplets. *Rev. Sci. Inst.*, **73,** 3988–3996

Yokoyama, E. 1993 Formation of patterns during growth of snow crystals. *J. Crystal Growth*, **128,** 251–257

Yokoyama, E. and Kuroda, T. 1990 Pattern formation in the growth of snow crystals occurring in the surface kinetic process and the diffusion process. *Phys. Rev. A*, **41,** 2038–2049